Ionics
DOI 10.1007/s11581-016-1968-7

ORIGINAL PAPER

Fading analysis of the Li(NiCoMn)O_2 battery under different SOC cycle intervals

Yiduo Zhu[1,2] · **Fuwu Yan**[1,2] · **Jianqiang Kang**[1,2] · **Changqing Du**[1,2] · **Chi Zhang**[1,2] · **Richard Fiifi Turkson**[3]

Received: 30 August 2016 / Accepted: 27 December 2016

Abstract In a review of literature on operating conditions, such as temperature, materials, cutoff voltage, and current rate, state-of-charge (SOC) interval has attracted less attention regarding research on cell fading. Lithium-ion cells as power source practically applied to electric vehicles (EVs) are seldom operated in the entire SOC interval, which means that lithium-ion cells are employed in a certain SOC interval. However, the SOC interval that facilitates the increase of the life span of the cell remains unknown. In the current study, several cells are tested over different SOC intervals and discharge rates. In-depth analysis is performed on the influence of the two factors on cell fading. The incremental capacity and incremental resistance methods are used to analyze capacity fading and resistance evolution. The electrochemical mechanism analysis of cell fading is studied and discussed, showing that SOC interval influences the rate of cell degradation. Results show that a low SOC interval prolongs the life span of cell use if other operating conditions are similar. Therefore, the study provides a theoretical framework and reference for the cell maintenance of EVs.

Keywords Incremental capacity · Interval cycle · Loss of lithium inventory · Loss of active material

✉ Jianqiang Kang
kjqiang@whut.edu.cn

[1] Hubei Key Laboratory of Advanced Technology for Automotive Components, Wuhan University of Technology, Wuhan 430070, China

[2] Hubei Collaborative Innovation Center for Automotive Components Technology, Wuhan University of Technology, Wuhan 430070, China

[3] Mechanical Engineering Department, Ho Polytechnic, P.O. Box HP 217, Ho, Ghana

Introduction

With the improvement of environmental protection consciousness on the part of people, electric vehicles (EVs) are gaining popularity. EVs need cell state and fault information to ensure safe operation. Compared with the state-of-charge (SOC) of the cell, the study of state-of-health (SOH) has recently become a subject of research. SOH and cell degradation are closely interrelated. Some studies have been conducted recently on cell fading. These studies can be divided into different categories, including theoretical analysis, modeling, mechanism, and operating conditions. Among these categories, the effect of operating conditions on cell fading is now becoming a topic of research interest, thereby providing direct information for formulating a strategic framework for EVs.

The degradation of lithium-ion batteries is determined by several factors, such as temperature, type of materials, cutoff voltage, current rate, and cycle interval. Yi [1] investigated the effect of storage temperatures on the kinetics of lithium ion use for the construction of cell positive electrodes via electrochemical impedance spectroscopy. Gao [2] prepared a type of NCM cell and studied the characteristics of the voltage special capacity curves for different charging/discharging rates. Rate capability and cycle performance at certain current rates were demonstrated. The evolution of differential capacity versus voltage in cycles was also studied. Liao [3] synthesized a series of spinal $LiNi_xMn_{2-x}O_4$ ($0 \le x \le 0.5$) with a varying ratio of Ni/Mn. Findings in the study [3] revealed that with an increase in the ratio of Ni/Mn, the capacity of the 4.0-V plateau decreases, the capacity of the 4.7-V plateau increases, and the total discharge capacity increases. Dubarry and Liaw

Published online: 14 January 2017

[4, 5] investigated the degradation mechanism of a composite $\{LiMn_{1/3}Ni_{1/3}Co_{1/3}O_2 + LiMn_2O_4\}$-based Li-ion cell using the electrochemical inference approach established by an incremental capacity (IC) analysis. IC peak indexed by convoluting the four positive electrode (PE) reactions with the five negative electrode (NE) reactions demonstrated. Berecibar [6] extensively studied and compared three commonly used supervised learning methods for SOH estimation in a nickel manganese cobalt (NMC) oxide cell. The evolution of capacity, IC, and differential voltage curves in terms of aging were researched. Bloom [7] tested several NMC cells for calendar and cycle life at 60% SOC in different temperatures and concluded that the *C*/25 capacity decreased with the square root of time. Schmalstieg [8] constructed numerous cells at different temperatures, various SOCs, and different cycle durations. The resulting fitting functions include the dependency of capacity and resistance on time, respectively, charge throughput, and other various parameters.

Apart from experimental studies, studies on capacity fading modeling of lithium-ion battery were also conducted. Wu [9] developed a dynamic model with parameters updated in real time. An incremental analysis-based autoregressive exogenous modeling method was verified in urban dynamic driving sequence profiles. Zhou [10] found a linear correlation between mean voltage falloff (MVF) and capacity. Thereafter, MVF was used as a novel health indicator (HI) for battery degradation modeling and the prediction of the remaining useful life (RUL). An optimized relevance vector machine was also employed to predict the RUL based on the presented HI. Zhou [11] proposed a novel approach for RUL prognosis. The approach combined empirical mode decomposition and autoregressive integrated moving average model. Su [12] systematically examined seven principal factors using an orthogonal design of experiments. An empirical aging model was introduced, followed by deceleration factor for comparing the fading capacity under different test conditions. Wu [13] presented an online approach using the feed-forward neural network (FFNN) and importance sampling (IS) to estimate lithium-ion battery RUL. The relationship between RUL and charge curve was simulated by FFNN, and IS was employed for FFNN input selection. Wang [14] constructed a state-space model for the lithium-ion battery capacity to assess capacity degradation. A spherical cubature particle filter was introduced to solve the state-space model.

A review of studies on cell degradation showed that experimental studies focus on the effects of temperature, current rates, cutoff voltage, depth of discharge or charge, and the ratio of Ni/Mn on cell fading, whereas the studies on the capacity fading modeling of lithium-ion battery aim to find a correlation between capacity degradation and operating conditions. However, research on the relationship between SOC interval and cell fading is insufficient. Commercial batteries, which serve as a power source applied to EVs, are seldom operated in the entire SOC interval (0–1). Batteries are seldom discharged or charged completely in a real operating condition. However, the interval favorable to extend the cell life span remains unknown. In this study, several lithium-ion cells are tested for life cycles in different SOC intervals. This study aims to seek the law of the effect of SOC interval on cell degradation. Results from this study will help in the foundation of the strategy frame for battery management system, which can prolong the cell life span.

Experimental setup

$Li(NiCoMn)O_2$ cylindrical 18650 lithium-ion batteries that are commercially available were provided by the Tianjin Lishen Battery Company. The PE material is $Li(NiCoMn)O_2$, and the NE material is graphite. Table 1 shows the cell parameters. The multichannel test equipment (model number CT4008) was provided by the Tianjin Neware Electronics Company. The test temperature controlled by environmental chambers was stable at 25 °C. The reference performance test (RPT) was used in accordance with the USABC test protocol [15], including the capacity test, hybrid pulse power characteristic test, and the IC test.

Table 2 is a matrix of the cycle aging test. In the matrix, SOC = (0,0.3) implies that the cell is cycled in the SOC range of 0–0.3 until the capacity loss reaches 20% through the following steps: the cell is discharged entirely under *C*/3, charged under a constant current (CC) at *C*/2 to 30% SOC, and thereafter discharged under 1C or 2C to the cutoff voltage of 2.75 V. Similarly, SOC = (0.4,0.7), SOC = (0.7,1), and SOC = (0,1) also imply that the cell is cycled in the given range until 20% capacity is consumed by conducting the following steps: the cell is charged entirely using the standard CC/CV, discharged under 1C or 2C to 40, 70, and 0% SOC, and charged under *C*/2 to 70, 100, and 100% SOC, respectively. The RPT test was carried out after every 50 cycles for SOC = (0,1) and 150 cycles for others. The SOC ranges of 0–0.3, 0.4–0.7, and 0.7–1 represent the lower, middle, and upper

Table 1 Cell specification based on the data sheet

Nominal capacity	2,600 mAh (at 0.2C discharge)
Minimum capacity	2,520 mAh (at 0.2C discharge)
Charging voltage	4.20 ± 0.05 V
Average working voltage	3.70 V at 0.2C
Standard charge method	Constant current/constant voltage (CC/CV)
Maximum charge current	0.5C (1300 mA)
Maximum discharge current	2C (5200 mA)
Cycle life	300th cycle ≥80% of 1st capacity (0.5C/1.0C at 25 °C)

Table 2 Matrix of the cycle aging test

Cell number	Cycle interval	Discharge rate	Cycle count
1	SOC = (0,0.3)	1C	4200
2	SOC = (0,0.3)	2C	4200
3	SOC = (0.4,0.7)	1C	4200
4	SOC = (0.4,0.7)	2C	4200
5	SOC = (0.7,1)	1C	4050
6	SOC = (0.7,1)	2C	2850
7	SOC = (0,1)	1C	550
8	SOC = (0,1)	2C	450

intervals, respectively. The division of SOC intervals heavily relies on the rate of solid electrolyte interface (SEI) reaction. The corresponding explanation will be provided in the "Analysis of capacity fading" section. The experiments not only carried out quantitative analysis but also identified which part of the SOC intervals is more detrimental in deep charge/discharge.

Results and discussion

Analysis of capacity fading

Figure 1 shows the evolution of the *V-Q* curves with cycles for #4 cell, and the discharging capacity was measured at *C*/3 rate. The discharging capacity and voltage plateau decreased with an increment in cycles, with the capacity loss accelerating in the latter stage of the cycles (cycles > 2000). A similar trend is also observed in the *V-Q* curves of other cells. The explanation will be discussed in a later section.

Figure 2 compares the capacity fading of #7and #8 cells. The cycle interval of each cell is the same for SOC ranging from 0 to 1, whereas the discharge rate in every cycle for the

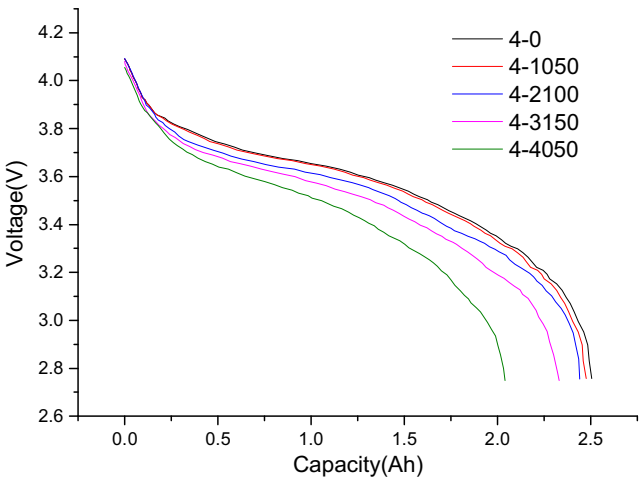

Fig. 1 *V-Q* curves of #4 cell as a function of cycle number at *C*/3 discharge

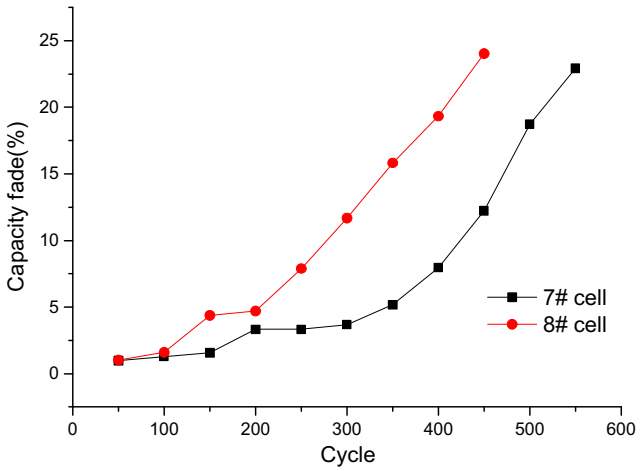

Fig. 2 Capacity fading comparison between #7 and #8 cells

#7 and #8 cells is 1C and 2C, respectively. The capacity fading curves of both cells overlap at the first 200 cycles. Thereafter, #8 cell capacity fading goes faster, wherein a high discharge rate accelerates capacity fading. A high current rate increases the polarization of the electrode potential in the PE or NE, accelerating the rate of the parasitic reactions and the changing of the active material structure. These factors further hasten cell degradation.

Figure 3 compares the capacity fading of #1–#6 cells. The discharge rate in every cycle of #1, #3, and #5 cells is 1C, whereas #2, #4, and #6 is 2C. Nos. 1 and 2 cell cycles can be noted in the lower SOC interval, #3 and #4 cell cycles are in the middle SOC interval, and #5 and #6 cell cycles occur in the upper SOC interval. The capacity decreases steadily when the cycles are less than 2000, thereby suggesting that the rate capability remains intact. The capacity loss accelerates and the rate capability worsens beyond 2000 cycles. In addition, the capacity fading rates are significantly different and their differences are considerably large when the cells are cycled in different SOC intervals (especially cycles > 2000). To conventionally compare the relative rate of the capacity fading, Table 3 shows the average capacity of fading per 100 cycles

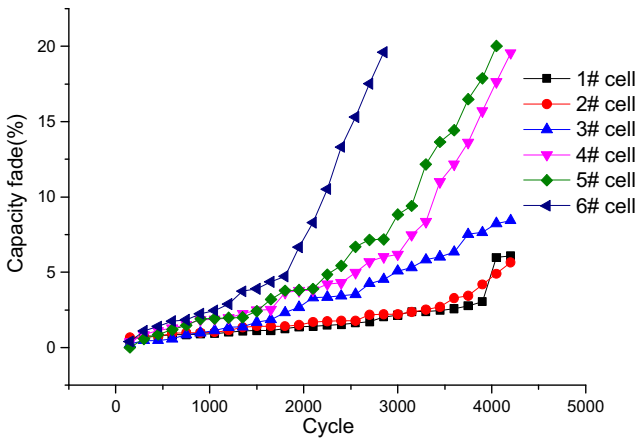

Fig. 3 Capacity fading comparison for #1~#6 cells

Table 3 Average capacity fading rate of the cells

Cell	#1	#2	#3	#4	#5	#6	#7	#8
Average fading capacity (%)	0.14	0.13	0.2	0.47	0.49	0.69	4.17	5.34

of all cells. Based on the results shown in Fig. 3 and Table 3, a high current rate evidently makes capacity fading faster even if the SOC interval is entirely the same. Furthermore, an upper SOC interval accelerates capacity fading even if the current rate is entirely the same. Compared with the #8 cell, the #4 cell had the same discharge rate and 1/3 SOC interval. However, the average capacity fading rate of #4cell is nearly 1/11 than that of #8 cell. The coupling relationship between SOC intervals and the current rate is also analyzed. Comparing #3 and #4 cells, the capacity fading rate of the latter is 2.35 times faster than that of the former owing to the influence of current rate. Comparing #3 and #5 cells, the capacity fading rate of the latter is 2.45 times faster than that of the former owing to the influence of SOC intervals. Comparing #3 and #6 cells, the capacity fading rate of the latter is 3.45 times faster than that of the former owing to the coupling influence of SOC intervals and current rate.

A SEI reaction is one of the major factors that degrade lithium-ion cells. Our previous work [16] has proven that the rate of SEI formation is closely related to SOC. If the SOC is higher than the threshold of 57%, the SEI reaction occurs even when the battery is at rest (i.e., in open circuit). With the increasing of the current, the SOC threshold at which SEI reaction occurs may move down below 40% owing to a polarization effect. Thus, SEI reaction in the interval of SOC = (0,0.3) does not exist, the SEI reaction is slow in the interval of SOC = (0.4,0.7), and the SEI reaction is enhanced in the interval of SOC = (0.7,1). This result explains clearly why the cell capacity fading becomes faster when it is cycled in the upper SOC interval even if the current rate is constant. In addition, the temperature is another major factor that leads to cell fading. The released heat is significantly larger for the cell that is cycled in the entire SOC interval than the partial SOC interval, as well as the temperature. Thus, the fading rate of the #7 and #8 cells is faster than that of others. Against the preceding background, capacity fading is evidently influenced by both the current rate and the SOC interval. The higher the current rate or the upper the SOC interval is, the faster the capacity fading becomes.

Analysis of the ohmic resistance evolution

Figure 4 shows the comparison of the charging and discharging resistance for #4 cell at 0.5 SOC, wherein the two curves show a similar trend. The discharging resistance is slightly higher than the charging resistance. In NE, the extraction hindrance of lithium in discharging is larger than the insertion hindrance in charging. Figure 5 shows a comparison between the charging resistance for #4 cell at 0.2, 0.5, and 0.8 SOCs. The internal resistance decreases with an increase in the SOC (except SOC = 1). References [17–20] have explained such phenomena in which the higher the voltage is, the lower the resistance becomes. Figure 6 shows the charging and discharging incremental resistance for #4 cell compared at 0.2, 0.5, and 0.8 SOCs. The incremental resistance ($\Delta R/R_0$, where R_0 is the initial resistance) is evidently independent on the SOC. Thus, the resistance measured at different SOCs is averaged for analyzing the incremental resistance.

Figure 7 compares the incremental resistance of #7 and #8 cells. The two curves are slightly different. Tan [17] explained why the effect of current rate of the resistance is insignificant: with the cell internal temperature rising, the internal resistance decreases, thus leading to less heat in the next period and ultimately achieving a relatively dynamic balance. The higher the current rate is, the more heat is generated; the higher the cell internal temperature is, the lower the resistance is. Thus, a higher current rate slows down resistance evolution. This condition is the reason why a current rate has a slight influence on the resistance shown in Fig. 7, which is different from the trend of the capacity shown in Fig. 2. Thus, when the heat predominates cell fading, the influence of the current rate on the resistance is unobvious.

Figure 8 compares the incremental resistances of #1–#6 cells. The trend of the curves in Fig. 8 is similar to the capacity fading curves shown in Fig. 3. Both the cycle interval and the discharging current rate have obvious effects on the incremental resistance. Based on the electrochemical mechanism analysis [21–26], the increase in resistance is attributed to the loss of active material (LAM) and the development of SEI. In

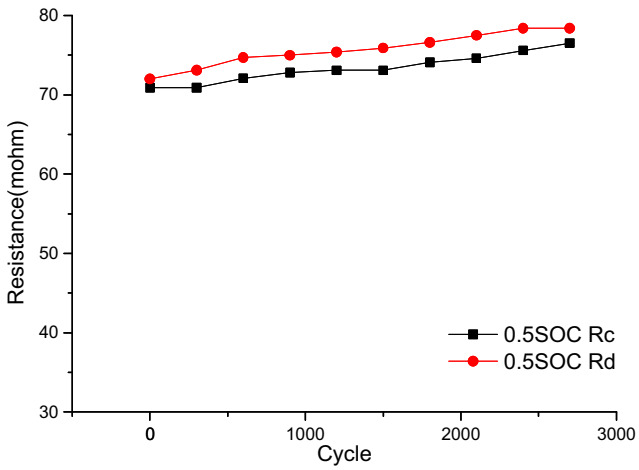

Fig. 4 Comparison of charging and discharging resistance for #4 cell at 0.5 SOC

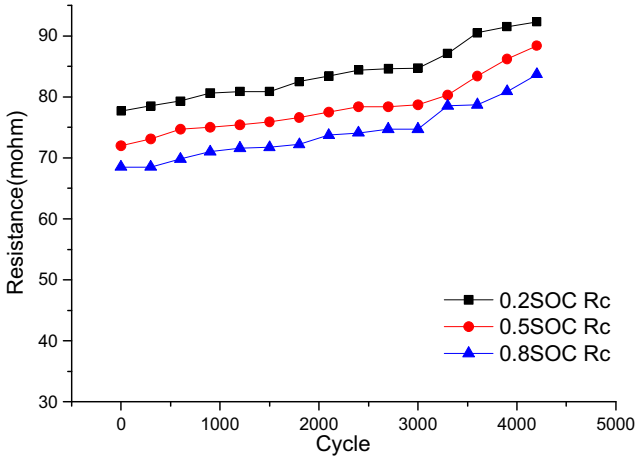

Fig. 5 Comparison of charging resistance for #4 cell at SOC = 0.2, 0.5, and 0.8

addition, the probability of the SEI reaction is larger in the upper SOC interval than in other SOC intervals. The parasitic reaction notably leads to electrolyte oxidation and the development of a lithium salt on the SEI. Owing to the difficulty in penetrating the solid state of lithium salt, the effect is equivalent to the increase in resistance.

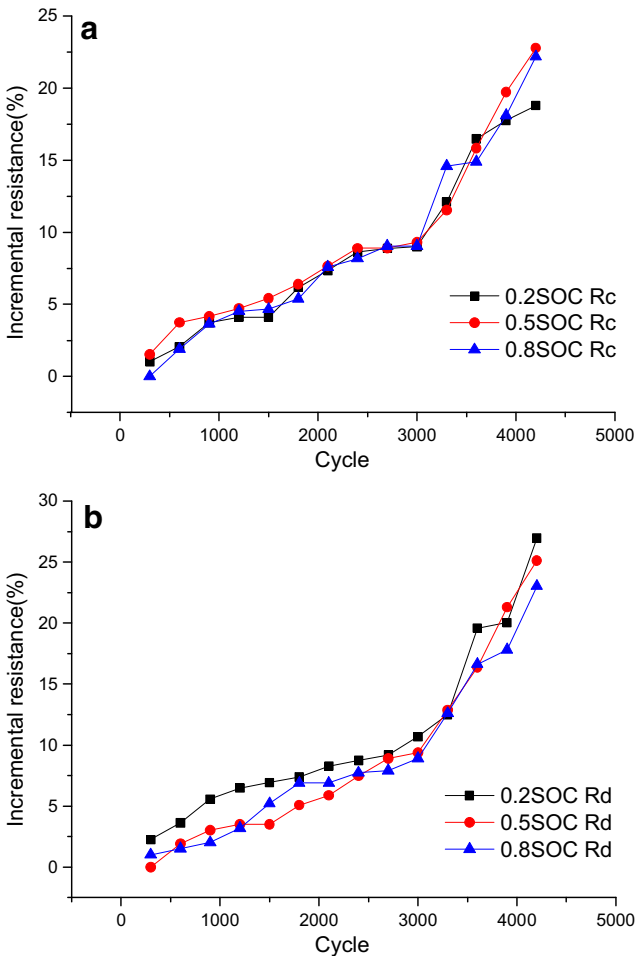

Fig. 6 Comparison of incremental resistance for #4 cell at SOC = 0.2, 0.5, and 0.8. **a** Charging. **b** Discharging

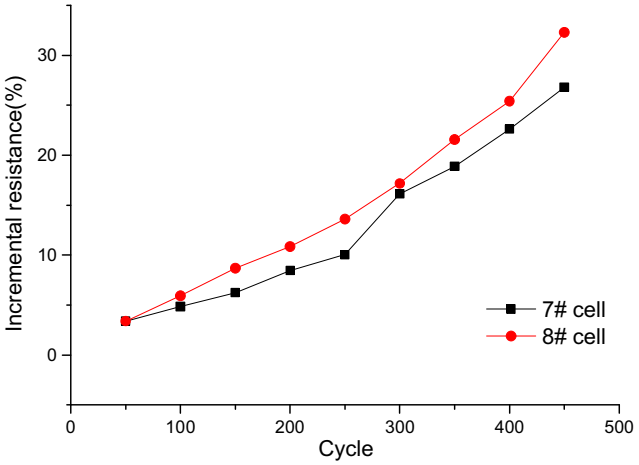

Fig. 7 Incremental resistance comparison between #7 and #8 cells

Comparing Fig. 8 with Fig. 3, the increase of internal resistance was found to accelerate when cell degradation reached a certain stage (cycles > 2000 for #3–#6 cells, cycles > 4000 for #1 and #2 cells). Heat generation significantly increases at a certain period, thereby accelerating fading. Therefore, the preceding discussion shows that the resistance evolution is influenced by both the current rate and the SOC interval. The higher the current rate or the upper the SOC interval is, the faster the resistance increases. However, the SOC interval should be a partial interval. For the entire SOC interval, the heat generated by the high current rate should be considered. The heat release is determined by both current rate and charge/discharge depth, which was clearly proven by our previous work [27].

Analysis of fading mechanism

The targeted cell chemistry in the current study employs a $Li(NiCoMn)O_2$ PE and a graphite NE. Based on the results

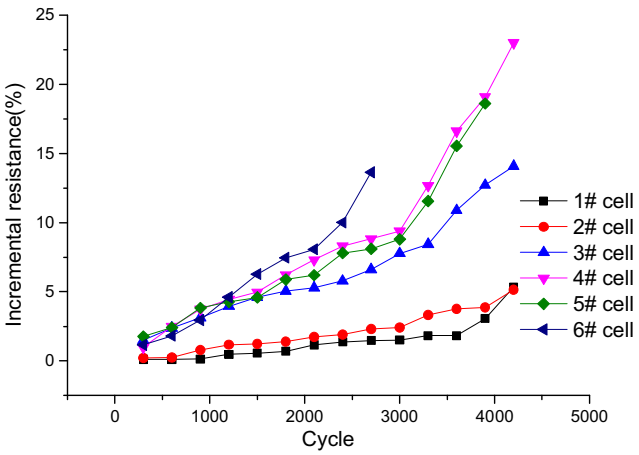

Fig. 8 Incremental resistance comparison among #1~#6 cells

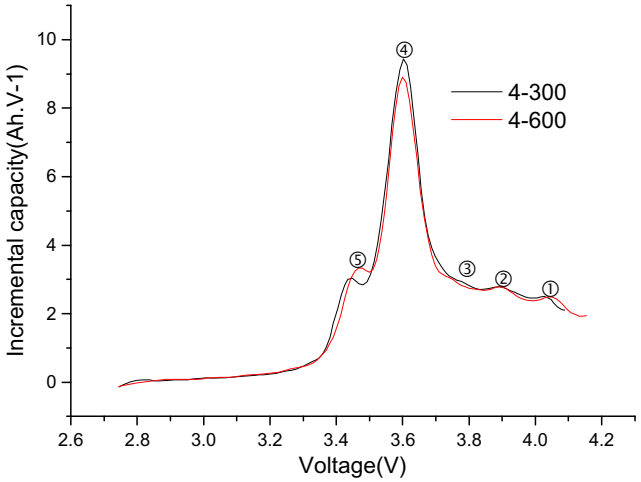

Fig. 9 IC curves of #4 cell after 300 and 600 cycles at *C*/25 discharge

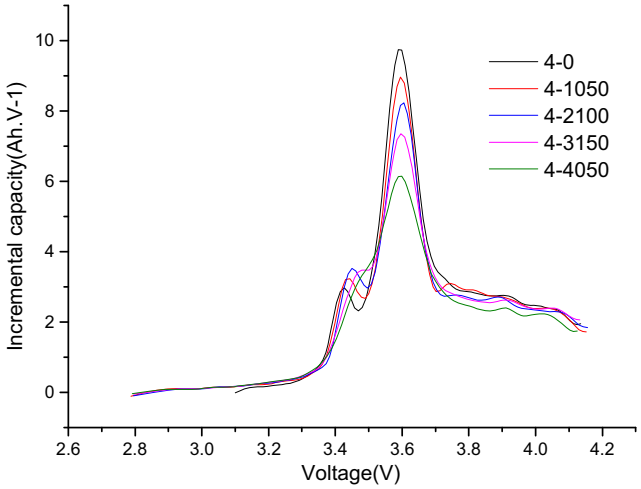

Fig. 10 IC curve of #4 cell after different cycles

drawn from references [4, 5], $Li(NiCoMn)O_2$ presents a steady potential decrease from 4.2 to 3.75 V in the solid-solution region in the hexagonal phase of the PE potential range. Furthermore, Li intercalation in the crystal structure leads to a phase transformation to the rock salt phase and exhibits a potential plateau at 3.75 V. In the NE, the lithiated graphite undergoes five distinct phase transformations. For the IC curve ($-dQ/dV = f(V_{cell})$), every IC peak is a unique representation of an NE reaction convoluting with a corresponding PE reaction. Figure 9 shows IC curves of #4 cell after 300 and 600 cycles at *C*/25 discharge. Five peaks can be recognized as denoted by ①, ②, ③, ④, and ⑤, in accordance with the voltage decrease, as shown in Fig. 9. The maximum peak intensity emerges approximately 3.6 V, indicating that the greatest redox reaction occurs at this point. Empirically, the reaction around 3.6 V is attributed to the character of chemical element Co [9, 28], which suggests that some $LiCoO_2$ is present in the PE material.

Comparing the two curves in Fig. 9, the intensity of ①, ②, and ③ is fairly stable in the initial stage of the cycles. The intensity of ④ decreases with the increase in cycles. Dubarry [4] explained that the decline is attributed to the loss of lithium inventory (LLI). Lithium is consumed by the (yet-to-be-identified) parasitic reactions; thus, the amount of Li returning to NE decreases in the charging regime. A slight increase is observed at peak ⑤ in the increment of the cycles. As a result of LLI, while the full capacity of PE reaction in the rock salt phase remains available, the remainder of the capacity that is not engaged in the reaction at ④ will then become available for ⑤, leading to an earlier onset and growing peak intensity, which is called a cascade effect.

Figure 10 shows IC curves of #4 cell after different cycles and further validates the cascade effect. According to reference [5], LAM is considered as another reason for capacity fading during the later stage of the aging cycles. A significant decrease of intensity of the peak ④ is observed. Apart from this condition, peak ⑤ nearly disappeared after 3150 cycles, which can be attributed to the retarded kinetics on the NE or the phase transformation on the PE. In addition, the IC curve

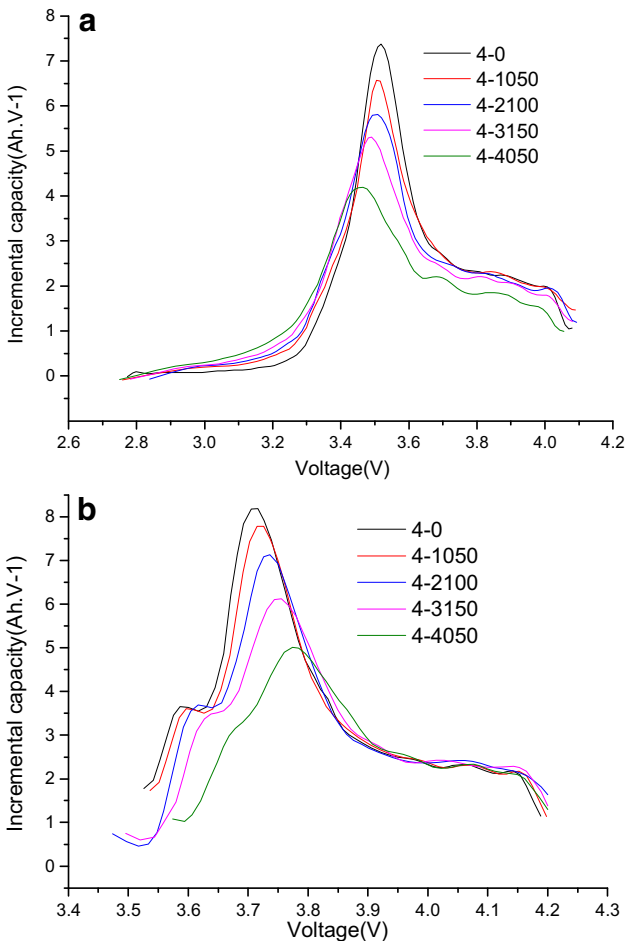

Fig. 11 IC curve of #4 cell after different cycles at **a** *C*/3 discharge and **b** *C*/3 charge

shows that the peak intensities of ①, ②, and ③ move down. In other words, the area under the curve with the given *x*-axis range (3.75–4.2 V) becomes gradually smaller with the increase in cycles. LAM is related to the dissolution of Mn in PE because the potential character of the chemical element Mn is around 4.0 V. Moreover, the kinetics of the spinal reaction is intact if the shape of peaks ①, ②, and ③ is not altered, suggesting that the LAM in the PE is possibly independent on the kinetics but is related to the dissolution of Mn [9, 29–31].

Figure 11a shows the IC curve of #4 cell after different cycles at *C*/3 discharge. Compared with the curve in Fig. 10, peak ⑤ disappears and peak ④ shows an earlier onset and a decrease in peak intensity. Figure 11b shows a later onset and a decreased peak intensity of peak ④, whereas the curve is fairly stable in the high-voltage region (above 3.75 V). By analyzing the effect of a current rate on the IC, the polarization effect is inferred to be responsible for the phenomena. The large polarization leads to a shifting of peak ④ and the disappearance of some peaks in the process of discharge. Further research is necessary to clarify the possible reasons. Consequently, IC curves of the samples in this study match well with the results plotted in references [4, 5]. Thus, the conclusions of Dubarry are used to explain the degradation of lithium-ion cell in the process of the cycles. LLI and LAM are the two main factors leading to cell degradation. The higher the current rate or the upper the SOC interval is, the more drastic the electrochemical reaction is.

Conclusions

Several cells were tested in this study for different SOC intervals and current rates. In-depth analysis was performed on the influence of the two factors on cell fading. Against the background of the preceding discussions, the following conclusions are drawn: (1) the upper SOC interval cycle causes faster capacity fading and resistance increase than other SOC interval cycle, (2) despite the effect of the cycle interval, a high current rate causes faster capacity fading and an increase in resistance, and (3) according to the electrochemical mechanism analysis, the LLI and LAM are the main reasons for the first two conclusions. The outcome of this research is considered in an SOH model associated with other influencing factors, such as temperature and depth of discharge; therefore, the SOH of the cell can be well predicted.

Acknowledgements This work was supported by the National Natural Science Foundation of China (NSFC) under grant numbers 51106115 and 51275367.

References

1. Zhu Y, Xie Y, Zhu R, Shu J, Jiang L, Qiao H, Yi T (2011) Kinetic study on $LiFePO_4$-positive electrode material of lithium-ion battery. Ionics 17:437–441
2. Gao J, Huang Z, Li J, He X, Jiang C (2014) Preparation and characterization of $Li_{1.2}Ni_{0.13}Co_{0.13}Mn_{0.54}O_2$ cathode materials for lithium-ion battery. Ionics 20:301–307
3. Wan R, Luo R, Liu Z, Tan X, Zhiyong F, Shijun L (2014) Effect of Ni/Mn ratio on the performance of $LiNi_xMn_{2-x}O_4$ cathode material for lithium-ion battery. Ionics 20:1361–1366
4. Dubarry M, Truchot C, Cugnet M, Liaw BY, Gering K, Sazhin S, Jamison D, Michelbacher C (2011) Evaluation of commercial lithium-ion cells based on composite positive electrode for plug-in hybrid electric vehicle applications. Part I: initial characterizations. J Power Sources 196:10328–10335
5. Dubarry M, Truchot C, Liaw BY, Gering K, Sazhin S, Jamison D, Michelbacher C (2011) Evaluation of commercial lithium-ion cells based on composite positive electrode for plug-in hybrid electric vehicle applications. Part II. Degradation mechanism under 2 C cycle aging. J Power Sources 196:10336–10343
6. Berecibar M, Devriendt F, Dubarry M, Villarreal I, Omar N, Verbeke W, Van Mierlo J (2016) Online state of health estimation on NMC cells based on predictive analytics. J Power Sources 320: 239–250
7. Bloom I, Walker LK, Basco JK, Abraham DP, Christophersen JP, Ho CD (2010) Differential voltage analyses of high-power lithium-ion cells. 4. Cells containing NMC. J Power Sources 195:877–882
8. Schmalstieg J, Käbitz S, Ecker M, Sauer DU (2014) A holistic aging model for Li(NiMnCo)O2 based 18650 lithium-ion batteries. J Power Sources 257:325–334
9. Wu H, Yuan S, Zhang X, Yin C, Ma X (2015) Model parameter estimation approach based on incremental analysis for lithium-ion batteries without using open circuit voltage. J Power Sources 287: 108–118
10. Zhou Y, Huang M, Chen Y, Tao Y (2016) A novel health indicator for on-line lithium-ion batteries remaining useful life prediction. J Power Sources 321:1–10
11. Zhou Y, Huang M (2016) Lithium-ion batteries remaining useful life prediction based on a mixture of empirical mode decomposition and ARIMA model. Microelectron Reliab 65:265–273
12. Laisuo S, Zhang J, Wang C, Zhang Y, Li Z, Yang S, Jin T, Ma Z (2016) Identifying main factors of capacity fading in lithium ion cells using orthogonal design of experiments. Appl Energy 163: 201–210
13. Wu J, Zhang C, Chen Z (2016) An online method for lithium-ion battery remaining useful life estimation using importance sampling and neural networks. Appl Energy 173:134–140
14. Wang D, Yang F, Tsui K-L, Zhou Q, Bae SJ (2016) Remaining useful life prediction of lithium-ion batteries based on spherical cubature particle filter. IEEE Trans Instrum Meas 65:1282–1291
15. Electric vehicle battery test procedures manual, U.S. Advanced Battery Consortium (USABC) and U.S. Department of Energy (US DOE), Idaho National Laboratory (INEEL), Revision 2, January 1996
16. Zhao P, Li M, Kang J, Rizzoni G (2017) Analysis of fading characteristics of a lithium ion battery based on an integration model. Int J Heat Mass Transf 104:1317–1324
17. Tan X (2011) Electric vehicle power battery management system design. Zhongshan University Press, Zhongshan
18. Wei S, Jiuchun J, Yanru Z, Yang Y, Yaojuan D, Weiping D (2015) Capacity fading and degradation mechanism of A123 battery. Power System Technology:1000–3673
19. Kitada K, Murayama H, Fukuda K, Arai H, Uchimoto Y, Ogumi Z, Matsubara E (2016) Factors determining the packing-limitation of

active materials in the composite electrode of lithium-ion batteries. J Power Sources 301:11–17

20. German F, Hintennach A, LaCroix A, Thiemig D, Oswald S, Scheiba F, Hoffmann MJ, Ehrenberg H (2014) Influence of temperature and upper cut-off voltage on the formation of lithium-ion cells. J Power Sources 264:100–107
21. Shuang L, Xiong L, He C (2014) Long cycle life lithium ion battery with lithium nickel cobalt manganese oxide (NCM) cathode. J Power Sources 261:285–291
22. Han X, Ouyang M, Lu L, Li J (2014) A comparative study of commercial lithium ion battery cycle life in electric vehicle: capacity loss estimation. J Power Sources 268:658–669
23. Nayak PK, Grinblat J, Levi M, Aurbach D (2014) Electrochemical and structural characterization of carbon coated $Li_{1.2}Mn_{0.56}Ni_{0.16}Co_{0.08}O_2$ and $Li_{1.2}Mn_{0.6}Ni_{0.2}O_2$ as cathode materials for Li-ion batteries. Electrochim Acta 137:546–556
24. Sankarasubramanian S, Krishnamurthy B (2012) A capacity fade model for lithium-ion batteries including diffusion and kinetics. Electrochim Acta 70:248–254
25. Baihua Zhang, Man Chen, Daiming Yang (2014) Investigation of the polarization effect in lithium iron phosphate battery for electric vehicles. Transportation Electrification Asia-Pacific (ITEC Asia–Pacific). 2014 I.E. Conference and Expo IEEE 1–5
26. Anitha Sarah Subburaj, Stephen B. Bayne (2014) Analysis of dual polarization battery model for grid applications. Telecommunications Energy Conference (INTELEC), 2014 I.E. 36th International, IEEE 1–7
27. Kang J, Rizzoni G (2014) Study of relationship between temperature and thermal energy, operating conditions as well as environmental factors in large-scale lithium-ion batteries. Int J Energy Res 38:1994–2002
28. Yang Gao, Caiping Zhang, Qiujiang Liu, Yan Jiang, Weiqiang Ma, Yong Mu (2014) An optimal charging strategy of lithium-ion batteries based on polarization and temperature rise. Transportation Electrification Asia-Pacific (ITEC Asia–Pacific),2014 I.E. Conference and Expo, IEEE 1–6
29. Weng C, Cui Y, Sun J, Peng H (2013) On-board state of health monitoring of lithium-ion batteries using incremental capacity analysis with support vector regression. J Power Sources 235:36–44
30. Cui Y, Chunyu D, Yin G, Gao Y, Zhang L, Guan T, Yang L, Wang F (2015) Multi-stress factor model for cycle lifetime prediction of lithium ion batteries with shallow-depth discharge. J Power Sources 279:123–132
31. Manikandan P, Periasamy P, Jagannathan R (2014) Grain boundary driven capacity fade/hysteresis abated in composite cathode material for lithium-ion batteries pouch cell. J Power Sources 264:299–310